Lower plate deformation at the Chile Triple Junction from the paleomagnetic record (45°30'-46° S)

Yves Lagabrielle, Jacques Bourgois, Jerôme Dyment, Bernard Pelletier

RESEARCH ARTICLE

Key Points:
- The SCR recorded remote and long-term effects of ridge subduction
- Volcanism has a link with abnormal subduction stress field
- Tectonic anomalies may be correlated with slab fragmentation

Correspondence to:
Y. Lagabrielle,
yves.lagabrielle@univ-rennes1.fr

Lower plate deformation at the Chile Triple Junction from the paleomagnetic record (45°30′S–46°S)

Yves Lagabrielle[1], Jacques Bourgois[2], Jerôme Dyment[3], and Bernard Pelletier[4]

[1]Géosciences Rennes, UMR 6118, Université de Rennes 1, Rennes CEDEX, France, [2]Sorbonne Universités, UPMC Université Paris 06, CNRS UMR 7193, Institut des Sciences de la Terre Paris, Paris, France, [3]Institut de Physique du Globe de Paris, CNRS UMR 7154, Sorbonne Paris Cité, Université Paris Diderot, Paris, France, [4]IRD, Nouméa, New Caledonia

Abstract During the Chile Triple Junction (CTJ) cruise, geophysical surveys were conducted between 45°S and 48°S, in the region of the Chile Triple Junction (CTJ), where the Nazca and Antarctica Plates are subducting beneath the South American Plate. Near the CTJ, the South Chile Rise (SCR), which separates the Nazca and Antarctica lower plates, consists of three spreading segments trending ~N160°, separated by a series of parallel fracture zones. The active spreading centers of the three segments consist of grabens with various widths and depths, bounded by steep fault scarps. We provide robust data showing that the SCR recorded remote and long-term effects of ridge subduction far from the subduction front. Magnetic profiles, multibeam bathymetric, and seismic data were acquired at intervals of 13 km along a N80°E direction across the SCR during the CTJ cruise of R/V *L'Atalante*. Deformation of the oceanic lithosphere includes (1) a segmentation of the spreading axes along strike, (2) some ridge jumps, and (3) local constriction and changes in trend of the fracture zone valleys. Off-axis volcanism is observed in places that may suggest a link with an abnormal stress field induced by ridge subduction. The tectonic and volcanic anomalies, which occurred in response to the subduction of the SCR1 axis, may be correlated with geochemical anomalies and slab fragmentation recognized by previous works.

1. Introduction

The Chile Triple Junction (CTJ) is the site where the South Chile Rise (SCR), the active spreading center separating the Antarctica and the Nazca Plates, is currently entering the subduction zone beneath the South American Plate [*Forsythe and Nelson*, 1985; *Cande and Leslie*, 1986; *Cande et al.*, 1987; *Bangs et al.*, 1992; *Behrmann et al.*, 1994; *Bourgois et al.*, 1996, 2000]. This region provides the unique opportunity to investigate the geological interactions between an actively subducting spreading ridge and a continental margin at a ridge trench-trench triple junction (Figure 1). The subduction of the SCR beneath the South American Plate is associated with a major change in the tectonic regime of the continental margin, since the margin undergoes subduction-erosion followed by subduction-accretion in response to the migration of the CTJ to the north [*Murdie et al.*, 1993; *Behrmann et al.*, 1994; *Bourgois et al.*, 1996, 2000]. Investigations conducted onshore and offshore in the region of the CTJ already revealed that important tectonic-magmatic interactions occur between the downgoing oceanic lithosphere and the overriding continental lithosphere, over the buried active spreading center. These interactions include tectonic coupling [*Bourgois et al.*, 1996; *Lagabrielle et al.*, 2000], emplacement of ophiolitic slices at 5.6 Ma [*Veloso et al.*, 2005; *Anma et al.*, 2006, 2009], and the emplacement of a wide variety of magma types including granites in the vicinity of the trench [*Mpodozis et al.*, 1985; *Forsythe et al.*, 1986; *Lagabrielle et al.*, 1994; *Bourgois et al.*, 1992, 1993, 1996; *Le Moigne et al.*, 1996; *Guivel et al.*, 1999, 2003; *Anma et al.*, 2009]. Until now, tectonic interactions in the CTJ region have been mostly documented based on geological data obtained from the upper continental plate or from investigations in the trench itself. Recently, effects of the subduction of the spreading center have been considered along the SCR away from the triple junction [*Blackman et al.*, 2012]. In this paper, we describe the structure and the tectonic evolution of spreading segments and transform faults of the SCR located close to the subduction front. Our set of marine data includes the results of a bathymetric and geophysical survey of the SCR obtained during the CTJ cruise of the R/V *L'Atalante* in 1997 [*Bourgois et al.*, 2000]. These data complement the extensive works recently conducted ashore from the continental side that provide valuable pieces for disentangling the feedback
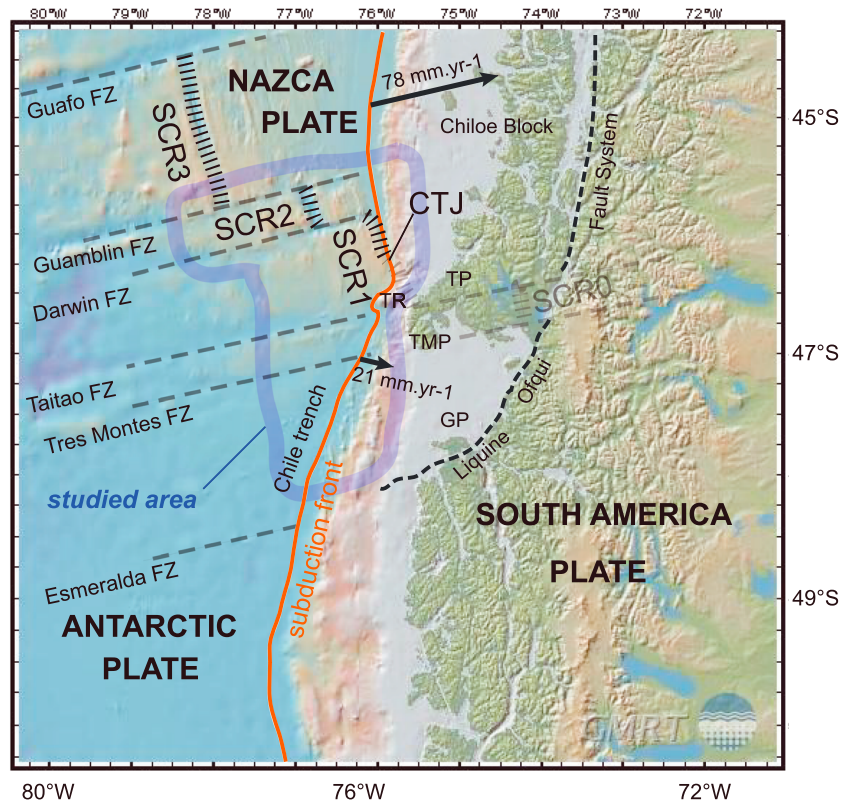
Figure 1. Location map of the CTJ area surveyed during the CTJ cruise of the R/V *L'Atalante* (Chief Scientist, J.B.). Vectors according to plate model NNR-MORVEL56 [*Argus et al.*, 2011].

coupling relationship between the upper and lower plates [*Mpodozis et al.*, 1985; *Forsythe et al.*, 1986; *Bourgois et al.*, 1996, 2000; *Lagabrielle et al.*, 2000; *Anma et al.*, 2006, 2009; *Blackman et al.*, 2012].

2. Subduction of the SCR and Geodynamical Evolution of Southern Patagonia

The average full spreading rate along the SCR (Figure 1) has been 62 mm/yr over the past 6 Ma [*Tebbens et al.*, 1997]. Because the ridge axis is trending 10° oblique to the orientation of the trench, the triple junction migrates northward (at ~160 km/Ma) when in a ridge-trench-trench configuration [*Cande et al.*, 1987]. Conversely, when in a transform-trench-trench configuration, the CTJ migrates slowly southward. According to kinematic reconstruction [*Forsythe et al.*, 1986], a long segment of the SCR, which is segmented by three small-offset fracture zones (FZs), intersected with the Chile trench west of Tierra del Fuego around 14 Ma ago. Three short ridge segments were then subducted: the first one, south of the Golfo de Penas at 10 Ma; the second segment between the Esmeralda and the Tres Montes FZ at 6 Ma, west of the Golfo de Penas; and the third one, between the Tres Montes and Taitao FZ at 3 Ma, west of the Tres Montes Peninsula. The segment of the ridge between the Taitao and the Darwin FZs is presently being subducted and intersects the trench at 46°09′S. Therefore, along the Patagonian margin, the subducting oceanic lithosphere exhibits a pervasive segmentation including three short segments between the Guamblin and the Tres Montes FZ and two longer segments located to the north and to the south of these fracture zones, respectively.

3. An Overview of the Results of the CTJ Cruise

The CTJ cruise of R/V *L'Atalante* (March–April 1997) investigated the structure and petrology of both the continental and oceanic lithospheres in the CTJ region, offshore Patagonia. A geophysical survey including Simrad EM12 multibeam echo sounding, sonar imagery, six-channel seismic reflection, gravity, and magnetic profiling was conducted between 45 and 48°S. A 100% coverage bathymetric map was

obtained covering the oceanic crust, the trench, and the inner wall of the subduction zone [*Bourgois et al.*, 2000]. Volcanic and sediment samples were recovered from numerous dredge sites located in the vicinity of the Chile Triple Junction, both on the oceanic and the continental sides [*Guivel et al.*, 2003]. The CTJ cruise took place after Ocean Drilling Program (ODP) Leg 141, during which five sites were drilled along the Chile continental margin. Sediments recovered during ODP Leg 141 are Quaternary to early Pliocene clays, gravels, and conglomerates, the oldest sediments being dated at 4.2–4.3 Ma [*Behrmann et al.*, 1992, 1994].

A clear segmentation of the Andean continental margin related to the migration of the CTJ is observed from the geometry of the Chile Trench [*Bourgois et al.*, 2000]. The continental margin north of the Darwin FZ, from 45°10′S to 45°50′S, is typical of subduction margin architecture before the subduction of the Chile Ridge. This "presubduction segment" is characterized by a thick trench infill currently underthrusted beneath a narrow continental slope. Between 45°50′S and 47°10′S, a more complex segment is regarded as the "synsubduction segment." The typical "postsubduction segment," located south of 47°10′S, exhibits a wide accretionary wedge (i.e., the Golfo de Penas accretionary prism) composed of a succession of parallel, compressional ridges in relation with active stacking of sedimentary slices.

No direct correlation exists between these three segments of the continental margin and the five segments (see following section) of the subducting oceanic plates. However, the uplifted synsubduction segment, which overlies the Chile Ridge at depth, exhibits very complex tectonic and magmatic signatures, suggesting a high coupling at depth between the spreading ridge and the continental margin. By contrast the presubduction and postsubduction segments exhibit less tectonic and magmatic complexity, suggesting a low degree of coupling between the subducting and overriding plates.

From previous interpretations of the CTJ cruise data it has been suggested that a very recent westward jump of the spreading center occurred along the segment currently entering the subduction zone [*Bourgois et al.*, 2000]. This clearly pointed to short-term instabilities within the oceanic lithosphere of the Chile Triple Junction, in addition to those in the upper plate, during the past 1–2 Ma period. Here we provide new robust data from magnetic profiling and structural analysis showing that the SCR indeed experienced remote and long-term effects of ridge subduction even far from the subduction front.

## 4. Structure of the Ocean Floor in the CTJ Region

4.1. Bathymetry of the SCR North of the CTJ

The SCR offshore southern Chile consists of spreading segments trending ~N160°, separated by a series of parallel fracture zones, from north to south: the Guamblin, Darwin, Taitao, and Tres Montes FZs (Figures 2 and 3). The segment of the SCR currently entering the Chile Trench is labeled SCR1. Both segments north of SCR1 are labeled SCR2 and SCR3. The axes of segments SCR1 and SCR3 are 37 km and 150 km long, respectively, and remarkably linear. By contrast, the axis of segment SCR2 is shorter, only 43 km long, and shows an internal segmentation. The length of the segment SCR1, which has partly entered the subduction zone, is estimated at 53 km, north of the CTJ. The tectonic-volcanic fabric of seafloor emplaced along the axis of segments SCR3 to SCR1 during the past 2–3 Myr exhibits different characteristics.

The axial valley of segment SCR3 (Figure 4) is roughly 15 km wide. The maximum depth of the axial seafloor reaches 3000 m while the flanks have an average depth of 2400 m. Linear ridges culminating at 2700 m are present within the axial depression. As shown by the imagery data, the neovolcanic zone corresponds to a wide field of small active volcanoes and lava flows occupying most of the axial seafloor (Figure 2b).

The axis of segment SCR2 is not linear (Figures 2a, 3, and 4) and is divided into three subsegments trending N170, N0, and N160, respectively. It shows typical deep nodal basins at both its southern and northern ends corresponding to the deepest points of the surveyed region (Figures 4a). The width of the axial graben varies from 15 to 5 km. The neovolcanic zone is defined by a N-S alignment of small volcanic cones and is better observed in the central subsegment. By contrast to segment SCR3, both walls of the axial valley of segment SCR2 are highly faulted and locally consist of successive steps, some hundreds of meters wide (Figure 5). Two domains of contrasting morphology, trending roughly E-W (labeled "sharp relief area" at Figure 4a), have been mapped to the west and to the east of the active axis. They show intense faulting and correspond to regions of uplifted oceanic crust (Figure 4a).
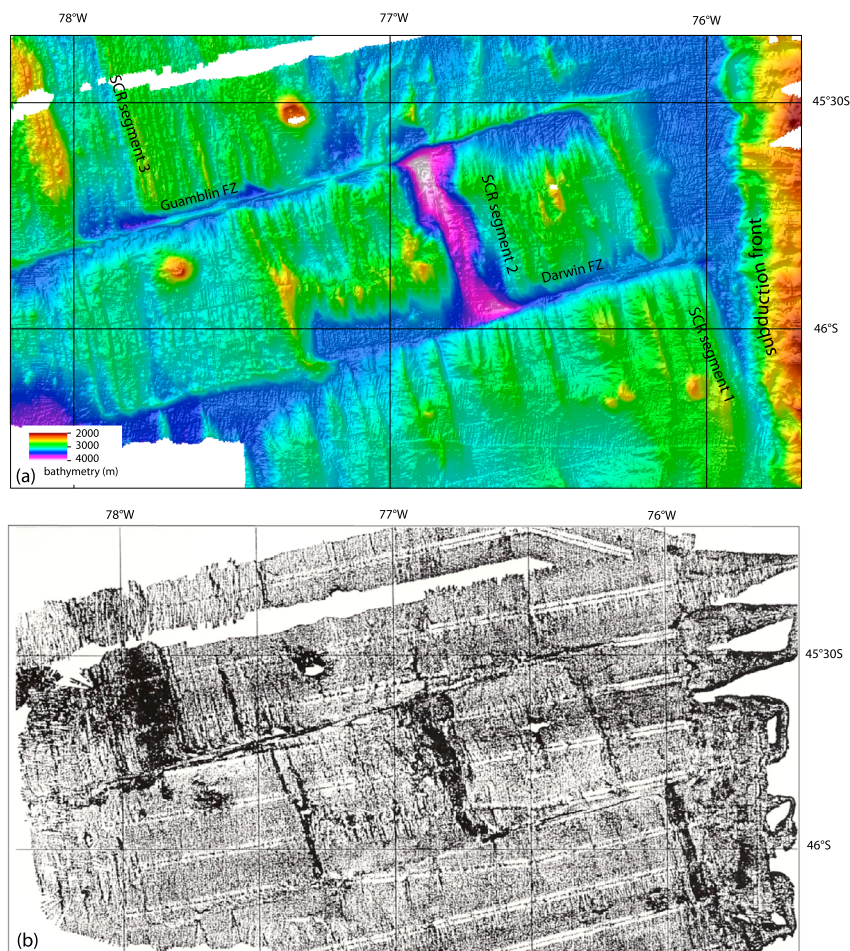
Figure 2. (a) EM12 bathymetry of the CTJ area surveyed during the CTJ cruise of the R/V *L'Atalante*. (b) EM12 imagery, note the high backscatter of the axial valleys of the three segments, in particular segment SCR1.
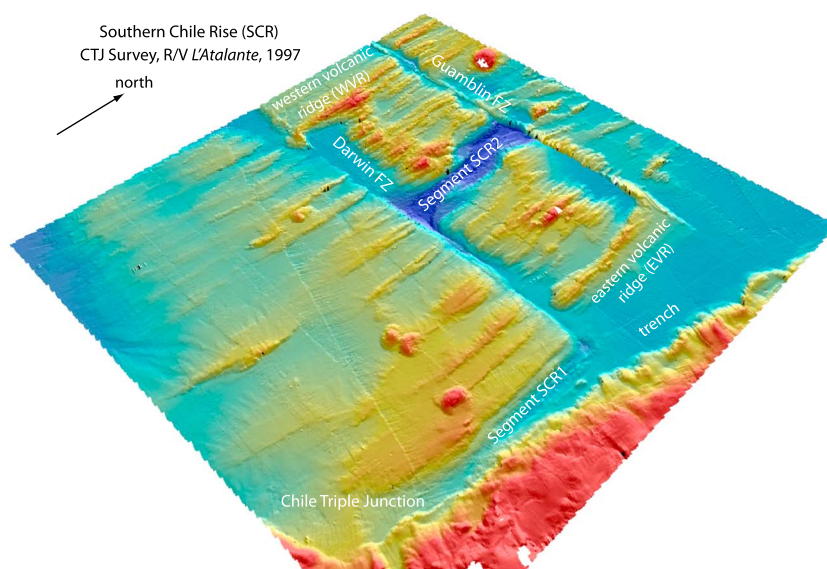

Figure 3. Three-dimensional bathymetric map derived from the EM12 bathymetric records. Oblique view from SE. See text for more details.

Figure 4. (a) Interpretation of the bathymetry of the northern part of the CTJ survey showing strong backscatter regions and main depressions. (b) Main volcanic fields, note the rifted volcanic ridges along segment SCR2. See text for more details.

Uplift occurred along N180 to N160 trending faults. Volcanic edifices are associated with the uplifted regions (Figure 4b). Domains of down-dropped crust are present near both transform faults in the SW and NE corners of the deformed regions. A large block of uplifted oceanic lithosphere bounded by the eastern volcanic ridge (EVR) (Figures 3 and 4) marks the eastern limit of the eastern deformed region. The EVR was probably emplaced at the ridge axis during a period of high magma supply. A similar ridge, the western volcanic ridge (WVR), is located symetrically on the western portion of segment SCR2 and bounds to the west a sharp relief area. Such symetrical locations suggest that both ridges have been rifted from a single axial ridge. To the north of the EVR, the western flank of the uplifted block curves into a narrow ridge, which connects to the Guamblin FZ. The southern boundary of segment SCR2 corresponds to the Darwin FZ. In the southwestern part of the mapped area, the fracture zone is not rectilinear as it could be expected for a nondeformed fracture zone (see section 4.3 below).

The axial valley of segment SCR1 is 10 km wide in its northern part and shows a relatively flat floor. Turbidites from the continental margin may have partly filled the axial depression. The western flank consists of two main steps (Figures 4 and 5) lying at 2600 m and 2800 m depth, respectively. Imagery data of the active zone do not show numerous volcanic cones as observed along other segments. Three recent off-axis volcanoes are aligned along the N80 direction south of the Darwin FZ (Figures 2–4). They might be considered as marking the southern boundary of a region of recently deformed and uplifted crust as suggested by the strong backscatter response. These data complement those published by *Blackman et al.* [2012], who have described in great detail the morphologic evolution along the axial zone, from segment 4 in the north to the Chile Triple Junction in the south, documenting a consistent pattern of clockwise rotation of the southernmost axial volcanic ridge within each of segments 2, 3, and 4, relative to the overall trend of the rift valley.
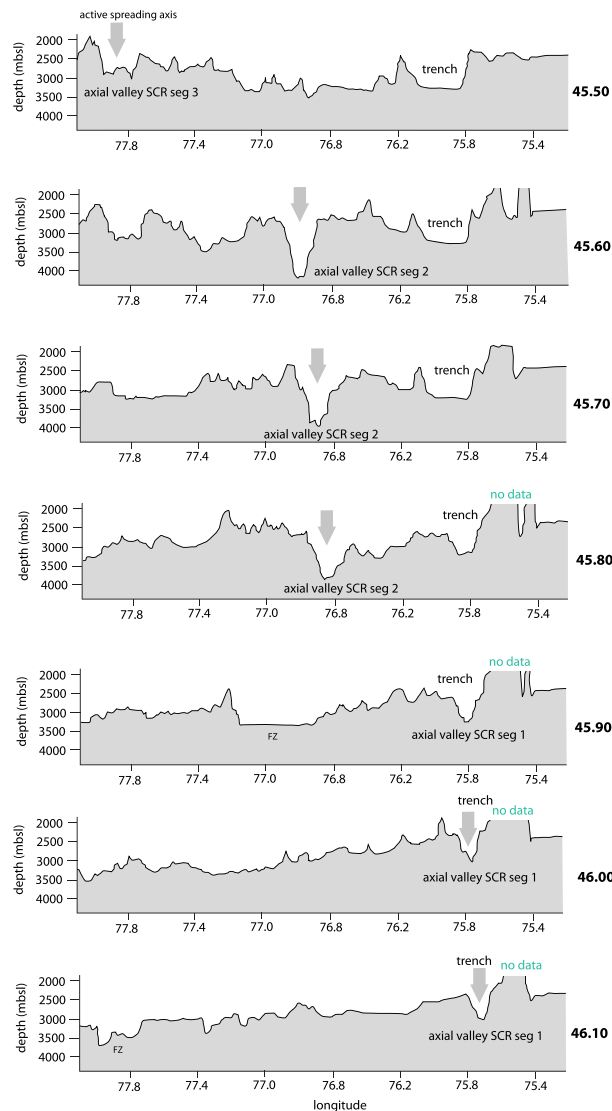
Figure 5. E-W topographic profiles across the bathymetric grid of the preridge subduction region.

4.2. Volcanoes and Anomalous Volcanic Ridges

A 20 km wide field of recent or active volcanoes is present to the west of the axis of segment SCR3 (Figures 4a and 4b), paralleling the active spreading axis. Volcanoes and associated lava flows are also present to the southern end of the active segment. Recent volcanic activity at these sites is documented by acoustic imagery data (Figures 2a and 2b). The fresh lava flows have erupted on the floor of the nodal basin, over the crust emplaced along segment SCR2. Because a deep morphologic low exists north of the lava field, sources of magmas are therefore located south of the Guamblin FZ, in unexpected positions for a "normal" segment boundary. A 10 km wide volcano is present at 77°40'W to the east of the axis of segment SCR3. The acoustic imagery reveals the presence of associated recent flows. Four N-S trending volcanic ridges have been recognized east of the volcano. Both ridges and volcanoes are roughly aligned along the direction of relative convergence of the Nazca and South American Plates. Segment SCR2 displays the largest volcano of the surveyed area. It also shows some kilometer-long fresh lava flows. The volcano exhibits a circular crater and inner cones and is located itself within a field of numerous smaller cones south of segment SCR3. East of this volcano, a long volcanic ridge paralleling the axial direction exhibits a dark, highly reflective signature on the acoustic imagery map. The northern segment of this ridge appears rifted and branches into two parallel ridges separated by a graben (profile 2, Figure 5) filled with sediment (Figure 2b). East of the SCR2 segment a major volcanic ridge exists (Figures 4a and 4b and CTJ3 profile at Figure 7). This ridge exhibits the same magnetic picks and isochrones than the volcanic ridge identified west of SCR2 (see section 5). Therefore, these volcanic ridges erupted at the same time during the anomaly 2 at about 2 Ma ago. These volcanic ridges are mirror images from one to the other. These data document that the volcanic ridge located east of SCR2 (CTJ3 profile, Figure 7) is a morphological seafloor feature, which developed along the SCR2 segment at about 2 Ma ago.
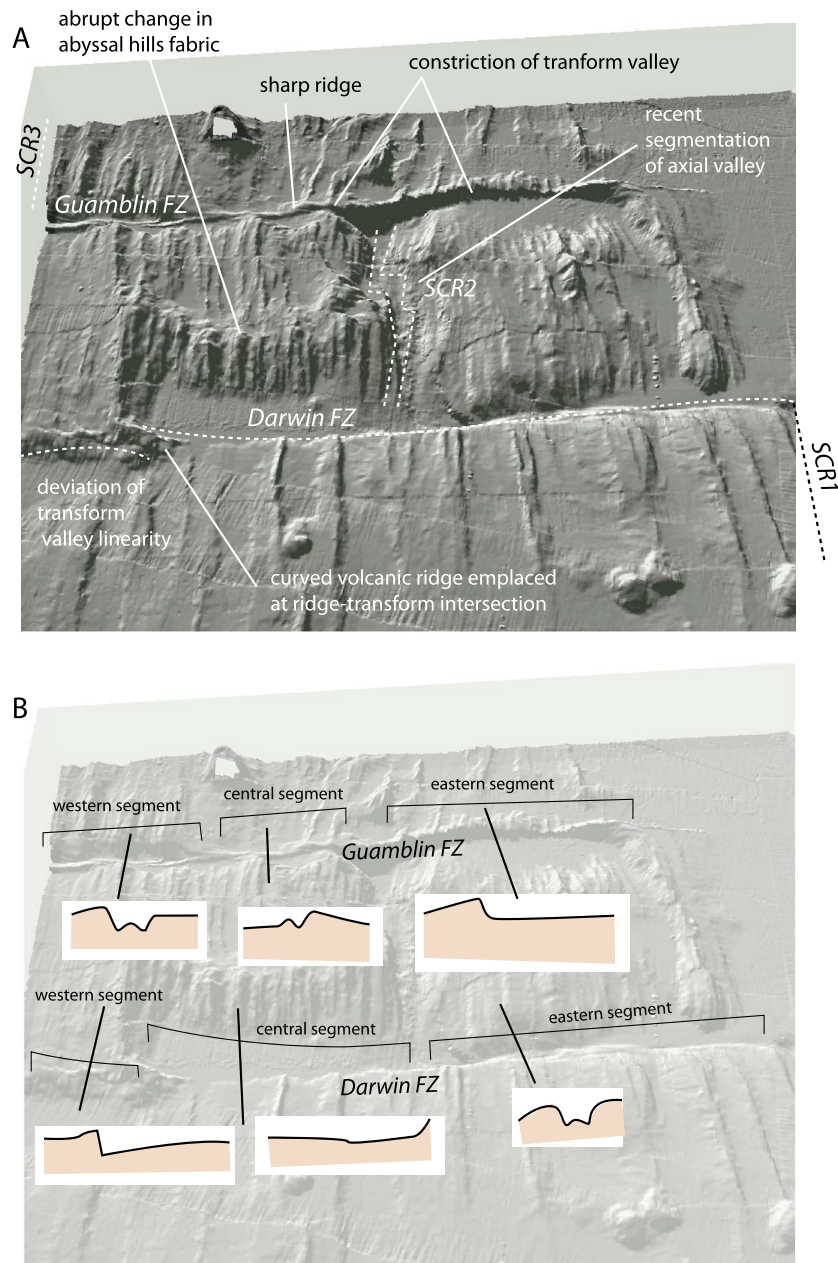
4.3. Deformation of Fracture Zones

Instead of being rectilinear as are fracture zones, the Guamblin and Darwin FZs show marked sinuosity and deformation. They exhibit a clear segmentation and variations of width and depth along strike, with contrasting morphological cross profiles (Figure 6). They can be divided into segments defined by various trends and differences in depth and width of their central valleys.

The Guamblin FZ can be divided into three segments, from west to east: (1) The Western segment (78°10'S–77°30'W) trending N70°E is 55 km long. It shows typical fracture zone morphology, including a discontinuous

Figure 6. (a) Three-dimensional view of the acoustic imagery map of the CTJ survey covering the Guamblin and the Darwin FZ. (b) Morphologic profiles across FZ showing evidence for tectonic deformation. See text for more details.

median ridge. (2) The central segment, located between 77°30′W and 77°W, is 40 km long and trends N72°E. This segment is narrower and shallower than the western segment. A discontinuous median ridge is still observed, but the northern wall is not present. (3) The eastern segment is located between 77°W and the subduction front, it is 50 km long, and it trends N76°E. The whole segment presents a steep northern wall and is wider than the central one. By contrast to the former segments, the southern wall is not present and is replaced by a large sediment-filled depression. The segment ends with a curved shape and connects to the base of a sharp volcanic ridge parallel to the spreading axis direction.

The Darwin FZ can be divided into three segments as well: (1) the western segment runs with a curved shape from 78°10′W to the southern tip of the rifted volcanic ridge. (2) The central segment is disconnected from the western segment; its eastern end (77°58′W) corresponds to the southern limit of the large depression lying at
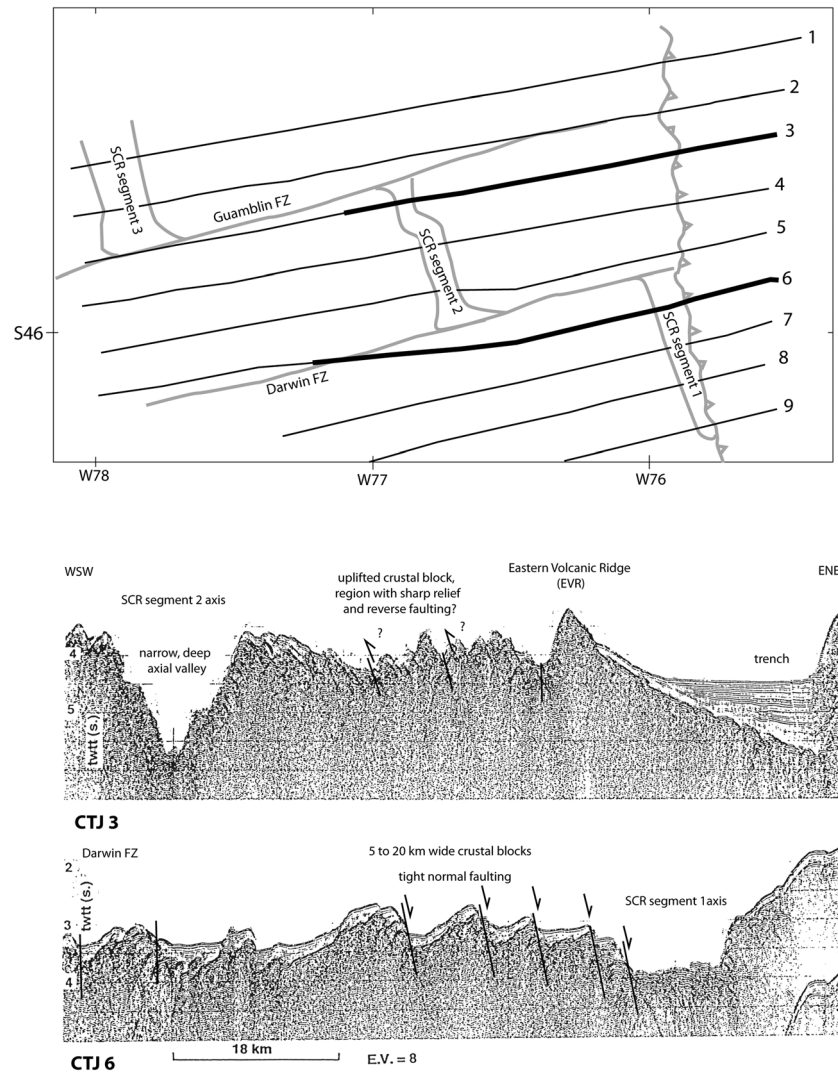
Figure 7. (a) Locations of reflection seismic lines along the presubduction region. (b) Two contrasting examples of seismic structures from the preridge subduction region. Profile CTJ3, note the thick sediment infill of the trench. Profile CTJ6, note the normal-faulting network west of the SCR1 segment. This was proposed as evidence of ridge jump along this ridge segment [*Bourgois et al.*, 2000].

the eastern foot of the rifted volcanic ridge. It also has a curved outline in plain view, but by contrast to the western segment, it is convex southward. It ends at its intersection with the SCR2 axial valley. (3) The eastern segment trends N72°E showing typical fracture zone morphology with two walls bounding a valley in which an irregular median ridge is observed. The eastern end presents a curved morphology.

Schematic bathymetric profiles perpendicular to the fracture zones (Figure 6b) show the variety in morphological types and their distribution along strike. In addition, it must be noted that the distance between the Guamblin and Darwin fracture zones decreases west of 77°30′W, suggesting shortening and deformation of the block located between them, west of the SCR2 axis. Two lines of evidence support the proposed interpretation. (1) The seafloor located between the SCR2 spreading center and the WVR is significantly uplifted (Figure 3), exhibiting an abrupt change in abyssal hill fabric and thus presenting a different morphology from the eastern portion of the segment (Figure 6). (2) Along the Guamblin FZ, the northern boundary of this region is a sharp ridge likely resulting from the constriction of the former transform valley (Figure 6). No connection exists between the "ridge and trough" morphologic signature of the seafloor located on either side of the sharp ridge. Seafloor hill crests on either sides of the ridge exhibit
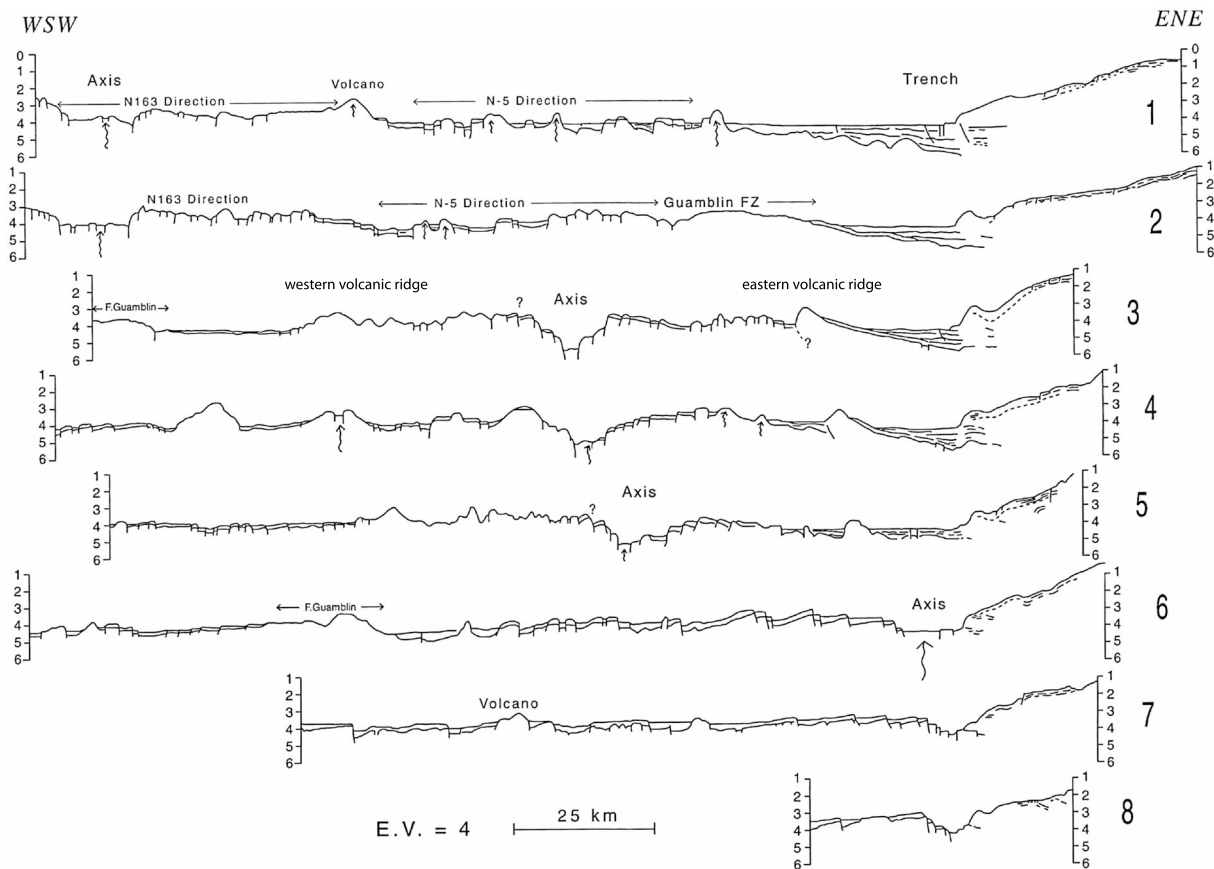
Figure 8. Line drawing of CTJ seismic lines 1 to 12.

bending that may be related to recent displacements. These features may result from clockwise rotations recently evidenced along the spreading segments [*Blackman et al.*, 2012].

4.4. Interpretation of Seismic Lines

Nineteen six-channel seismic reflection lines were collected during the CTJ cruise across the southern Chile margin in the area of the Chile Triple Junction (Figure 7). Line drawings of selected lines across the oceanic lithosphere (Figure 8) allow investigating the structure of the subducting plates. In general, the thickness of sediments covering the oceanic crust increases from north to south in relation to the transform faults and from east to west in relation to the proximity of the trench and the continent. The sedimentary cover is very thin in and around the axial valley of segment SCR3, north of the Guamblin FZ, in the northwestern corner of the surveyed area (westernmost part of profiles 1 and 2, Figure 8). East of this domain bounded by a volcano, the ocean floor is deeper and covered by 0.10 to 0.15 s thick sediments. As discussed in the following section on magnetic anomalies, this appears to result from a westward ridge jump. A more noticeable sedimentary thickness (0.20 to 0.30 s) is observed on the shoulders of the deep trough corresponding to the axial part of the segment 2, between the Guamblin and Darwin FZs (lines 3 to 5, Figure 8). The sediments are affected by normal faults, which face the trough. These sediments accumulated in half-graben structures exhibit thickening toward the base of the normal faults. East of the trough, the EVR prominent ridge corresponds to the top of an uplifted tilted block of oceanic basement draped by a 0.10 to 0.15 s thick sedimentary cover. The block tilted eastward together with its sedimentary cover is unconformably overlain by the horizontal trench-fill deposits (line CTJ3, Figure 7). This documents that the block has been tilted prior to enter the trench [*Bourgois et al.*, 2000]. The elevated region located between the trench and the SCR2 axis displays many faults, in relation with a marked fabric of the seafloor made of tight volcanic ridges. Such sharp relief may be related to numerous reverse faults, an interpretation consistent with the presence of the large tilted block on the eastern edge of this domain (Figure 7). These structures collectively suggest that this area suffered compression.
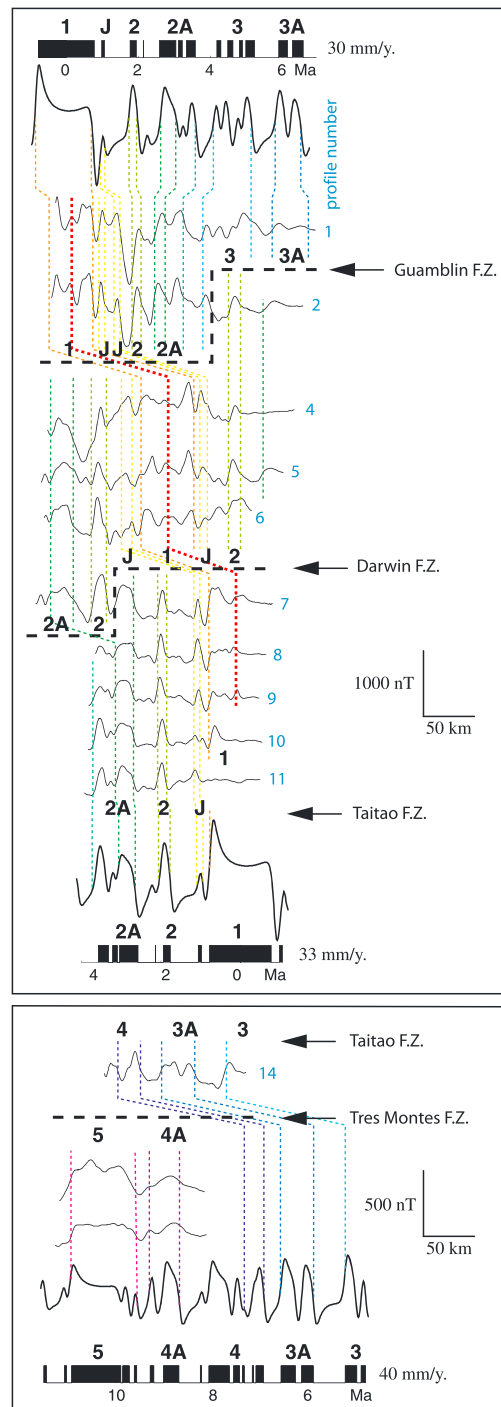
Figure 9. Interpretation of magnetic anomalies acquired during cruise CTJ. Thin lines: selected magnetic anomalies projected onto 80° profiles. Thick lines: synthetic magnetic anomalies, with geomagnetic polarity time scale (normal in black, with names; reversed in white), ages, and spreading rates. The colored dotted lines represent the magnetic isochrons, with different colors for different ages: red, ridge axis; orange, anomaly 1 (Brunhes period); yellow, anomaly J (Jaramillo event); light green, anomaly 2; dark green, anomaly 2A; light blue, anomaly 3; medium blue, anomaly 3A; dark blue, anomaly 4; purple, anomaly 4A; pink, anomaly 5. The dashed lines mark the locations of transform faults and fracture zones (with names), which interrupt the continuity of magnetic isochrons.

South of the Darwin FZ and west of the axis of segment SCR1, the oceanic crust and its 0.2 to 0.25 s thick sedimentary cover are tilted westward along normal faults facing the trench (line 6, Figure 7). These faults extend southward along lines 7 and 8 (not shown). Finally, the seismic reflection and magnetic data document oceanic crust deformation that occurred well before entering the subduction. Such evidence has to be added to the deformational features highlighted by our interpretation of the bathymetry, notably along the fracture zones.

5. Interpretation of Magnetic Data

During the CTJ cruise, 23 magnetic profiles (~3200 km of record) were acquired at intervals of 13 km along a N80°E direction, cutting across the SCR, almost parallel to the fracture zones, and oblique to the Chile Trench. These magnetic data, obtained together with the bathymetry, gravity, and seismic data, bring new constraints on the local plate motions. They also provide the opportunity to date the deformational events affecting the oceanic crust due to the subduction of the SCR. We have selected 13 magnetic anomaly profiles (Figure 9). They were projected along direction N80°E together with the corresponding synthetic magnetic anomaly model. The magnetic anomalies are identified by comparison of observed and modeled magnetic anomaly sequences. Magnetic anomalies 1 (axial anomaly, 0–0.78 Ma) to 5 (9.74–10.95 Ma) are identified in the study area. Ages are given according to the geomagnetic polarity time scale of *Cande and Kent* [1995]. The magnetic"-picks," which mark the crossing of our profiles with the magnetic isochrons of seafloor spreading in the survey area, are shown in map view with different symbols and colors (Figure 10). The red stars denote the ridge axis, marked by the Central Magnetic Anomaly High (CAMH) [*Klitgord*, 1976]. In general, the axial magnetic anomaly is made of three highs separated by two lows,
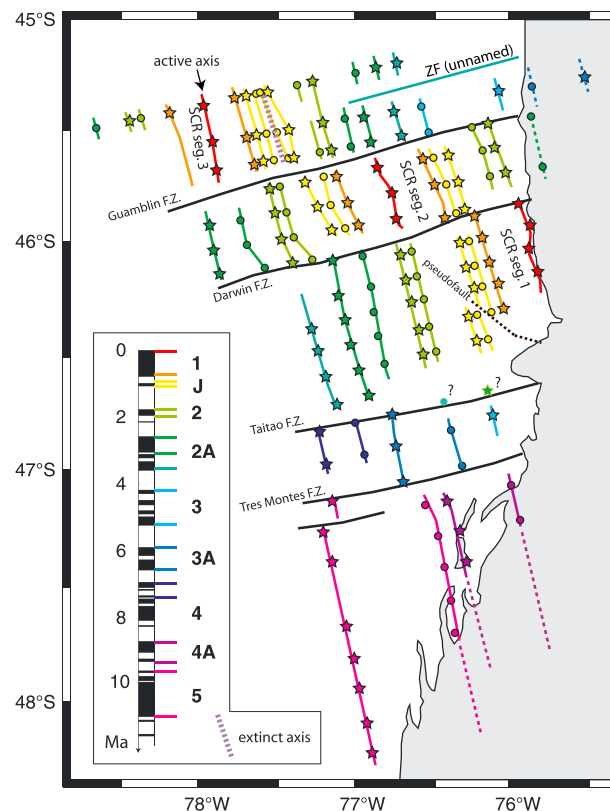
Figure 10. Magnetic picks, isochrons, and fracture zones deduced from the magnetic anomaly data acquired during CTJ cruise. The colored symbols and lines represent the magnetic picks and isochrons, with different colors for different ages (see inset for their ages and names). The stars (respectively, circles) mark the older (respectively, younger) side of normal polarity intervals. The black lines mark the locations of transform faults and fracture zones. The dotted lines denote the uncertain isochrons.

the central high being the CAMH. This pattern may reflect the variation of paleointensity within the Brunhes period [*Gee et al.*, 1996] or the effect of the axial valley bounding faults that facilitate seawater penetration and basalt alteration, thus lowering the magnetization [*Hussenoeder et al.*, 1996]. For other colors, circles denote the young side of the normal polarity blocks and stars their old side. "Warm" 273 colors correspond to younger age and "cold" colors to older ages. The isochrons are drawn between anomaly picks of same age. The fracture zones are identified from both the bathymetric and magnetic data (Figure 10). The younger anomalies (1 to 3A) in segments SCR1, SCR2, and SCR3 reveal a half spreading rate of 30 to 33 mm/yr, whereas the older ones (3 to 5) south of the Taitao FZ are consistent with a faster, ~40 mm/yr half spreading rate.

5.1. North of the Guamblin FZ

Our profiles across this region are mostly located on the eastern flank of the SCR (Figures 9 and 10). Only anomalies 2A (young side), 2, and 1 are observed on the western flank, with the Jaramillo anomaly missing. Conversely, the eastern flank exhibits anomalies 1, a doubled Jaramillo anomaly, 2, 2A, and 3. Anomaly 3A may also be present beneath the accretionary prism, beyond the trench. This anomaly pattern reveals a regular spreading, only interrupted by a minor, ~10 km westward jump of the ridge axis at about 0.9 Ma. At 77°20′W, the pronounced negative magnetic anomaly located immediately east of the double Jaramillo anomaly may be associated to a large seamount observed on the bathymetry (Figures 2–4 and 9).

5.2. North of the Darwin FZ

In this area, symmetrical magnetic anomalies J, 2, and 2A are identified on both side of the axial magnetic anomaly. The sediment thickness appears to be anomalous as compared to oceanic crust of the same age elsewhere (150 m associated with the Jaramillo event instead of less than 100 m) over such a young oceanic crust. The two volcanic ridges, which limit the deformed region of SCR2, are synchronous at about 2 Ma. Anomalies 2 and Jaramillo seem to split into three different segments (Figure 9), similar to the present "en echelon" morphology of the ridge axis (Figures 2–4). This observation suggests that the deformation may have affected the oceanic crust since chron 2 old (~2 Ma).
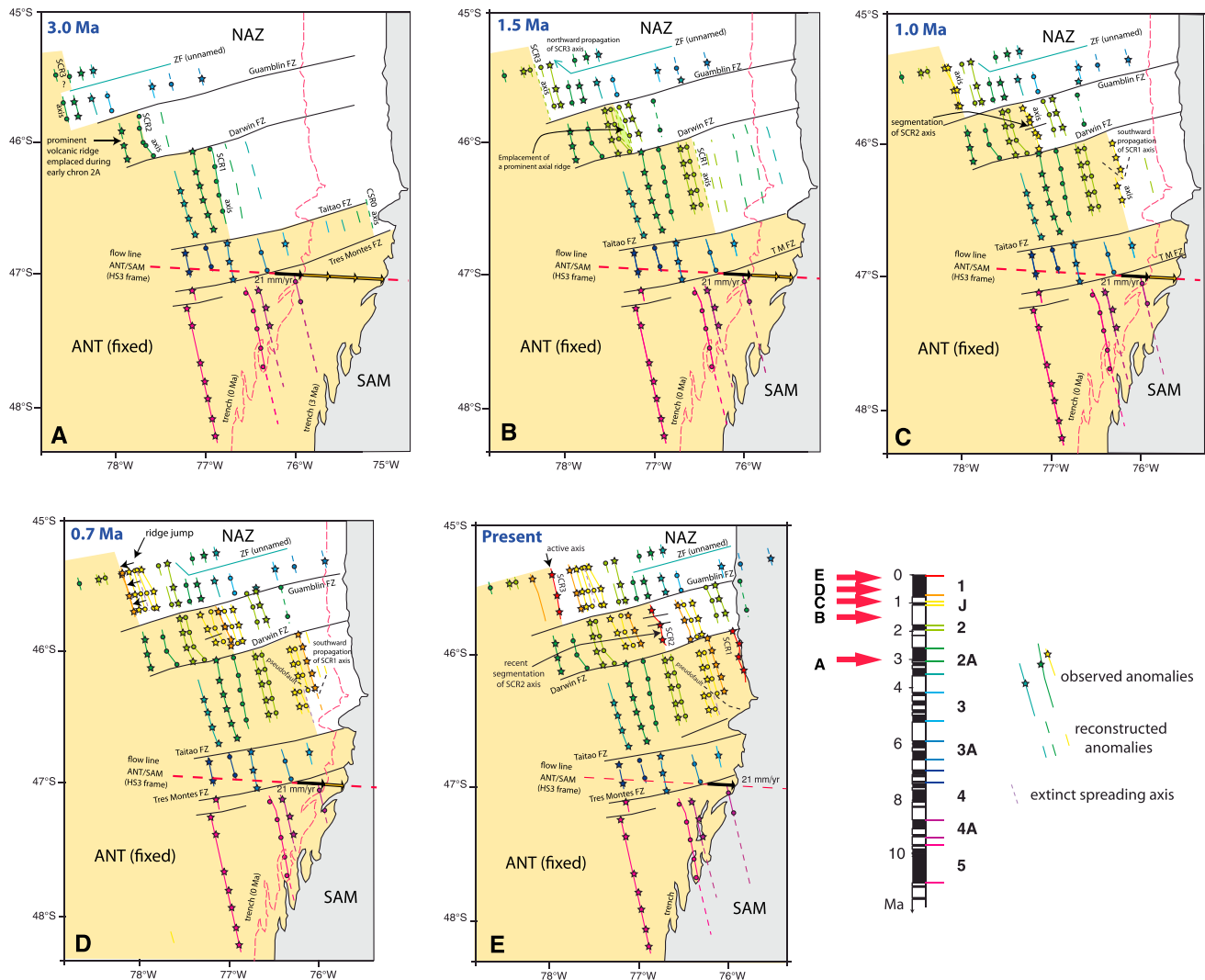
5.3. North of the Taitao FZ

This region only shows magnetic anomalies 1, J, 2, and 2A from the western flank of the SCR (Figures 9 and 10). A peculiarity of the region is the presence of a pseudofault associated with a southward verging propagating rift that cuts across most of the seafloor. This propagator initiated shortly after chron 2 (1.77 Ma) and offset the Jaramillo anomaly by about 10 km. On the eastern end of the profiles, the axial magnetic anomaly progressively decreases in amplitude and completely disappears south of 46°20′S, while the CAMH is only observed north of 46°10′S. Such 307 a pattern is also observed on other sedimented spreading centers such as the Middle Valley

Figure 11. Reconstruction of the relationship of the subducting oceanic plates—i.e., Nazca and Antarctica Plates—with the Chile continental margin for the past 3 Ma. Snapshots at (a) 3.0, (b) 1.5, (c) 1.0, and (d) 0.7 Ma, respectively. (e) Situation at present. Motion values are obtained through Submap and Okino 705 plate motions calculators (http://submap.gm.univ-montp2.fr/maps-index.php and http://ofgs.aori.u707tokyo.ac.jp/~okino/platecalc_new.html). The symbols and colors of magnetic picks and isochrones are the same as in Figure 10.

and other segments of the Juan de Fuca Ridge [*Currie and Davis*, 1994], basins in the Gulf of California [*Larson et al.*, 1972], and the eastern part of the Andaman spreading center [*Kamesh Raju et al.*, 2004]. Pervasive hydrothermal alteration or thermal demagnetization have been proposed to explain the lack of magnetic anomalies at these active spreading centers [e.g., *Levi and Riddihough*, 1986], but are hardly applicable to all these examples, which have in common an abundant sedimentation. An alternative explanation could be the lack of a significant basaltic extrusive layer.

5.4. South of the Taitao FZ

One of the profiles does not display identifiable magnetic anomaly (except at its western end where it shows anomalies 3 young and 2A old) as it follows the Taitao FZ on 80 km (Figure 10). Another one follows the Tres Montes FZ and barely shows anomaly 3A expressed north of Tres Montes FZ in its central part and anomaly 5 old expressed south of Tres Montes FZ on its western part. Other profiles show a regular succession of anomalies 4 to 3 old north of Tres Montes FZ, and anomalies 5 to 4A south of Tres Montes FZ, some of these anomalies being clearly expressed beneath the accretionary prism beyond the trench (Figures 9 and 10).

6. Discussion

Our interpretation of the magnetic anomalies (Figure 10) differs from those of *Cande and Leslie* [1986] and *Tebbens et al.* [1997], owing largely to our much larger number of magnetic picks. As reported in section 5 we identified ridge jump in compartment A, a propagator in compartment C, and curved isochrons in compartment B. The age of the subducting crust is, from south to north: (1) 9 Ma (anomaly 4A) in compartment E, south of Tres Montes FZ; (2) about 3 Ma (anomaly 3) in compartment D, between Taitao and Tres Montes FZ; (3) 0 Ma, i.e., the ridge is entering subduction, between Darwin and Taitao FZ, where the CTJ is located; (4) 2 Ma (anomaly 2) between Guamblin and Darwin FZ; and (5) 3 Ma (anomaly 3) north of Guamblin FZ. These ages confirm the northward migration of the Chile Triple Junction. Using these magnetic anomalies, we schematically reconstruct (Figure 11) the plate kinematics of this area at 0 (at present, Figure 11e), 0.7 (chron 1, Figure 11d), 1 (Jaramillo event, Figure 11c), 1.5 (interpolated between Jaramillo event and chron 2, Figure 11b), and 3 Ma (within chron 2A, Figure 11a). In this study, the most common values for the motion of the Chile Trench with respect to the Antarctic Plate have been used. A rate of 21 km/Ma in the direction of N93 has been retained according to the HS3 Pacific hot spot reference frame [*Gripp and Gordon*, 2002]. Similar values are obtained using the GSRM344 APM-1-Hotspot reference frame [*Kreemer*, 2009] and the NUVEL-1A models [*DeMets et al.*, 1994]. In the more recent NNR-MORVEL56 model [*Argus et al.*, 2011], the velocity is slightly greater (25 mm/yr). The motion of the Nazca Plate is reconstructed by superimposing the corresponding conjugate magnetic anomalies. These motions have been computed through Submap (http://submap.gm.univ-montp2.fr/maps-index.php) and Kyoko Okino's (http://ofgs.aori.u-tokyo.ac.jp/~okino/platecalc_new.html) plate motion calculators.

Based on our reconstructions, the evolution of the spreading center can be summarized as follows. At 3 Ma, the SCR0 axis collided with the trench at the locus of the present-day Taitao Ridge. At 1.5 Ma, a prominent axial ridge was emplaced at the SCR2 axis and extended within the nodal basins, where it adopted an arcuate shape. This ridge was split in two parts during the subsequent evolution. In the meantime, the SCR3 axis propagated northward and, as a result, the unnamed transform fault north of the Guamblin FZ became inactive. At 1 Ma, the southern part of the SCR1 axis collided with the South American Plate. This major event was associated with the initiation of a southward propagation of the SCR1 axis. In the meantime, the SCR2 axis was divided into two secondary segments. At 0.7 Ma, a ridge jump occurred on segment SCR3 and accretion ceased on the southern part of segment SCR1. Between 0.7 and 0 Ma, two discontinuities initiated at segment SCR3 which now consists in three small subsegments.

These reconstructions suggest that the ridge axis in compartment D—limited by the Tres Montes and Taitao FZ—has entered subduction shortly after 3 Ma. The deformation occurring in the area since the end of anomaly 2, in particular in compartment B, started after compartment D entered subduction, suggesting that the tectonic effects of ridge axis subduction are observed quite far (km) from the triple junction. Compartment D is short, and the effects of the progressive northward migration of the triple junction in this segment are relatively moderate. Conversely, when the twofold longer compartment C, limited by Darwin and Taitao FZ, begins to subduct and the triple junction again migrates northward for a longer time, intense deformation is observed in compartment B, located immediately north of this segment, since the end of anomaly 2. Large off-axis seamount affects an oceanic crust younger than 3 Myr.

7. Conclusion

Our magnetic data provide details for the evolution of the relationship between the subducting oceanic plates and the Chile continental margin for the past 6 Myr. The subducting SCR has recorded not only several degrees of the recent stress field rotation [*Blackman et al.*, 2012] but also progressive tectonic segmentation along some segments. (1) The seafloor north of the Guamblin FZ (Figure 10) exhibits a regular spreading since anomaly 3A, interrupted by an ~10 km westward jump of the ridge axis at about 0.9 Ma. (2) The seafloor south of the Guamblin FZ and north of the Darwin FZ (Figure 10) shows two volcanic ridges, which erupted during anomaly 2A. Subsequently, the SCR2 spreading center evolved through three short subsegments, which show an en echelon pattern associated with a clockwise rotation. Since anomaly 2A, this region evolved under an ~NS trending compressional tectonic regime in

agreement with the segmentation documented along the Guamblin and Darwin FZs. Moreover, the distance between the Guamblin and Darwin fracture zones decreases west of 77°30′W, suggesting shortening and deformation of the block located between them, west of the SCR2 axis. (3) The seafloor south of the Darwin FZ exhibits a propagator cutting across the whole compartment. This propagator initiated shortly after chron 2 (1.77 Ma) and offset the Jaramillo anomaly by about 10 km. Two different subsegments exist in this region: the SCR1a and SCR1b subsegments, the first one already subducted and the second one remaining to be subducted.

The data reported here are in line with the reconstruction of the ridge subduction history proposed for the SCR1 segment by *Bourgois et al*. [2000]. A westward jump of the SCR1 segment would have occurred during the past 780 kyr that produced slab fragmentation and individualization of the ephemeral Chonos microplate. Two episodes of subduction-accretion separated by an episode of subduction-erosion occurred in relation with the Chonos microplate individualization and subduction. Another ridge jump was proposed to have occurred at ~300–250 ka.

Finally, our data document pervasive tectonic disturbances related to ridge subduction. This is consistent with data previously collected in this region evidencing tectonic and geochemical interferences as the SCR approaches the Chile trench subduction [*Blackman et al*., 2012; *Klein and Karsten*, 1995]. The basalts recovered from the SCR1 segment have geochemical characteristics unlike those of mid-ocean ridge basalts sampled elsewhere. *Klein and Karsten* [1995] have shown affinities of these basalts with those from volcanic arcs. These observed chemical anomalies were interpreted to relate to contamination of depleted suboceanic mantle by marine sediments and altered oceanic crust.

These tectonic and geochemical anomalies most probably formed in response to the subduction of the SCR1 axis. One mechanism we invoke to explain these observations is small-scale sublithospheric convection (SSC) [*Schmerr*, 2012; *Ballmer et al*., 2007]. The privileged sites where SSC may occur at the Gutenberg discontinuity are regions where dynamical processes, including mantle convection and fluid release during subduction, strengthen melt production. We suggest that major anomalies in the CTJ area may originate from subduction-induced SSC allowing material from the upper plate to be recycled at the SCR spreading center.

References

Anma, R., R. Armstrong, T. Danhara, Y. Orihashi, and H. Iwano (2006), Zircon sensitive high mass-resolution ion microprobe U-Pb and fission-track ages for gabbros and sheeted dykes of the Taitao Ophiolite, southern Chile, and their tectonic implications, *Island Arc*, *15*, 130–142.

Anma, R., et al. (2009), Are the Taitao granites formed due to subduction of the Chile ridge?, *Lithos*, *113*, 246–258.

Argus, D. F., R. G. Gordon, and C. DeMets (2011), Geologically current motion of 56 plates relative to the no-net rotation reference frame, *Geochem. Geophys. Geosyst.*, *12*, Q11001, doi:10.1029/2011GC003751.

Ballmer, M. D., J. van Hunen, G. Ito, P. J. Tackley, and T. A. Bianco (2007), Non-hotspot volcano chains originating from small-scale sublithospheric convection, *Geophys. Res. Lett.*, *34*, L23310, doi:10.1029/2007GL031636.

Bangs, N., S. C. Cande, S. D. Lewis, and J. Miller (1992), Structural framework of the Chile margin at the Chile ridge collision zone, in *Proceedings of the Ocean Drilling Program*, *Initial Rep.*, vol. 141, pp. 11–21, Ocean Drilling Program, College Station, Tex.

Behrmann, J. H., et al. (1992), *Proceedings of the Ocean Drilling Program*, *Initial Rep.*, vol. 141, 708 pp., Ocean Drilling Program, College Station, Tex.

Behrmann, J. H., et al. (1994), Tectonics and geology of spreading ridge subduction at the Chile Triple Junction: A synthesis of results from leg 141 of the Ocean Drilling Program, *Geol. Rundsch.*, *83*, 832–852.

Blackman, D. K., B. Applegate, C. R. German, A. R. Thurber, and A. S. Henig (2012), Axial morphology along the Southern Chile Rise, *Mar. Geol.*, *315*, 58–63.

Bourgois, J., Y. Lagabrielle, R. Maury, J. Lemoigne, P. Vidal, J. M. Cantagrel, and O. Urbina (1992), Geology of the Taitao Peninsula (Chile Margin Triple Junction area, 46°–47°S): Miocene to Pleistocene obduction of the Bahia Barrientos ophiolite, *Eos Trans. AGU*, *73*(43), 592.

Bourgois, J., Y. Lagabrielle, J. Le Moigne, O. Urbina, M. C. Janin, and P. Beuzart (1993), Preliminary results of a field study of the Taitao ophiolite (southern Chile): Implications for the evolution of the Chile Triple Junction, *Ofioliti*, *18*, 113–129.

Bourgois, J., H. Martin, Y. Lagabrielle, J. Le Moigne, and J. J. Frutos (1996), Subduction erosion related to spreading-ridge subduction: Taitao peninsula (Chile Margin Triple Junction area), *Geology*, *24*, 723–726.

Bourgois, J., C. Guivel, Y. Lagabrielle, T. Calmus, J. Boulègue, and V. Daux (2000), Glacial interglacial trench supply variation, spreading-ridge subduction, and feedback controls on the Andean margin development at the Chile Triple Junction area (45-48°S), *J. Geophys. Res.*, *105*, 8355–8386, doi:10.1029/1999JB900400.

Cande, S. C., and D. V. Kent (1995), Revised calibration of the geomagnetic 532 polarity timescale for the Late Cretaceous and Cenozoic, *J. Geophys. Res.*, *100*(B4), 6093–6095, doi:10.1029/94JB03098.

Cande, S. C., and R. B. Leslie (1986), Late Cenozoic tectonics of the Southern Chile Trench, *J. Geophys. Res.*, *91*, 471–496, doi:10.1029/JB091iB01p00471.

Cande, S. C., R. B. Leslie, J. C. Parra, and M. Hobart (1987), Interaction between the Chile ridge and Chile trench: Geophysical and geothermal evidences, *J. Geophys. Res.*, *92*, 495–520, doi:10.1029/JB092iB01p00495.

Currie, R. G., and E. E. Davis (1994), Low crustal magnetization of the Middle Valley sedimented rift inferred from sea-surface magnetic anomalies, in *Proc. ODP, Sci. Results*, vol. 139, edited by M. J. Mottl et al., pp. 19–27, Ocean Drilling Program, College Station, Tex.

DeMets, C., R. G. Gordon, D. F. Argus, and S. Stein (1994), Effect of recent revisions to the geomagnetic reversal time scale on estimate of current plate motions, *Geophys. Res. Lett.*, *21*(20), 2191–2194, doi:10.1029/94GL02118.

Forsythe, R. D., and E. Nelson (1985), Geological manifestations of ridge collision: Evidence from the Golfo de Penas-Taitao Basin, southern Chile, *Tectonics*, *4*(5), 477–495, doi:10.1029/TC004i005p00477.

Forsythe, R. D., E. P. Nelson, M. J. Carr, M. E. Kaeding, M. Hervé, C. M. Mpodozis, M. J. Soffia, and S. Harambour (1986), Pliocene near trench magmatism in southern Chile: A possible manifestation of ridge collision, *Geology*, *14*, 23–27.

Gee, J., D. A. Schneider, and D. V. Kent (1996), Marine magnetic anomalies as recorders of geomagnetic intensity variations, *Earth Planet. Sci. Lett.*, *144*, 327–335.

Gripp, A. E., and R. G. Gordon (2002), Young tracks of hotspots and current plate velocities, *Geophys. J. Int.*, *150*, 321–361.

Guivel, C., Y. Lagabrielle, J. Bourgois, R. C. Mauryc, S. Fourcade, H. Martin, and N. Arnaud (1999), New geochemical constraints for the origin of ridge-subduction-related plutonic and volcanic suites from the Chile Triple Junction (Taitao Peninsula and Site 862, Leg ODP 141 on the Taitao Ridge), *Tectonophysics*, *311*, 83–111.

Guivel, C., Y. Lagabrielle, J. Bourgois, H. Martin, N. Arnaud, S. Fourcade, J. Cotten, and R. C. Maury (2003), Shallow melting of oceanic crust during spreading-ridge subduction: Origin of near-trench Quaternary volcanism at the Chile Triple Junction, *J. Geophys. Res.*, *108*(B7), 2345, doi:10.1029/2002JB002119.

Hussenoeder, M. A., T. H. Schouten, and R. C. Searle (1996), Near-587 bottom magnetic survey of the Mid-Atlantic Ridge axis, 24°-24°40′N: Implications for crustal accretion at slow spreading ridges, *J. Geophys. Res.*, *101*, 22,051–22,069, doi:10.1029/96JB01890.

Kamesh Raju, K. A., T. Ramprasad, P. S. Rao, B. Ramalingeswara Rao, and J. Varghese (2004), New insights into the tectonic evolution of the Andaman basin, northeast Indian Ocean, *Earth Planet. Sci. Lett.*, *221*, 145–162.

Klein, E. M., and J. L. Karsten (1995), Ocean ridge basalts with convergent margin geochemical affinities from the Chile ridge, *Nature*, *374*, 52–57.

Klitgord, K. D. (1976), Sea-floor spreading: The Central Anomaly Magnetization High, *Earth Planet. Sci. Lett.*, *29*, 201–209.

Kreemer, C. (2009), Absolute plate motions constrained by shear wave splitting orientations with implications for hotspot motions and mantle flow, *J. Geophys. Res.*, *114*, B10405, doi:10.1029/2009JB006416.

Lagabrielle, Y., J. Le Moigne, R. C. Maury, J. Cotten, and J. Bourgois (1994), Volcanic record of the subduction of an active spreading ridge, Taitao Peninsula (southern Chile), *Geology*, *22*(608), 515–518.

Lagabrielle, Y., C. Guivel, R. Maury, J. Bourgois, S. Fourcade, and H. Martin (2000), Magmatic–tectonic effects of high thermal regime at the site of active ridge subduction: The Chile Triple Junction model, *Tectonophysics*, *326*, 255–268.

Larson, P. A., J. D. Muddie, and R. L. Larson (1972), Magnetic anomalies and fracture zone trends in the Gulf of California, *Geol. Soc. Am. Bull.*, *83*, 3361–3368.

Le Moigne, J., Y. Lagabrielle, H. Whitechurch, J. Girardeau, J. Bourgois, and R. Maury (1996), Petrology and geochemistry of the ophiolitic and volcanic suites of the Taitao peninsula (Chile Triple Junction area), *J. South Am. Earth Sci.*, *9*, 43–58.

Levi, S., and R. P. Riddihough (1986), Why are marine magnetic anomalies suppressed over sedimented spreading centers?, *Geology*, *14*, 651–654.

Mpodozis, C. M., M. A. Hervé, C. Nasi, R. Forsythe, and E. Nelson (1985), El Magmatismo Plioceno de Peninsula Tres Montes y su relacion con la evolucion del Punto Triple de Chile Austral, *Rev. Geol. Chile*, *25–26*, 13–28.

Murdie, R., D. Prior, P. Styles, S. Flint, R. Pearce, and S. Agar (1993), Seismic responses to ridge transform subduction: Chile Triple Junction, *Geology*, *21*, 1095–1098.

Schmerr, N. (2012), The Gutenberg discontinuity: Melt at the lithosphere-asthenosphere boundary, *Science*, *335*, 1480–1483.

Tebbens, S. F., S. C. Cande, L. Kovacs, J. C. Parra, J. L. LaBrecque, and H. Vergara (1997), The Chile ridge: A tectonic framework, *J. Geophys. Res.*, *102*, 12,035–12,059, doi:10.1029/96JB02581.

Veloso, E., R. Anma, and T. Yamazaki (2005), Tectonic rotations during the Chile ridge collision and obduction of the Taitao ophiolite, southern Chile, *Island Arc*, *14*, 599–615.